Cell, Vol. 108, 357–369, February 8, 2002, Copyright ©2002 by Cell Press

Vacuole Fusion at a Ring of Vertex Docking Sites Leaves Membrane Fragments within the Organelle

Li Wang, E. Scott Seeley, William Wickner,[1] and Alexey J. Merz
Department of Biochemistry
Dartmouth Medical School
7200 Vail Building
Hanover, New Hampshire 03755

Summary

Three membrane microdomains can be identified on docked vacuoles: "outside" membrane, not in contact with other vacuoles, "boundary" membrane that contacts adjacent vacuoles, and "vertices," where boundary and outside membrane meet. In living cells and in vitro, vacuole fusion occurs at vertices rather than from a central pore expanding radially. Vertex fusion leaves boundary membrane within the fused organelle and is an unexpected pathway for the formation of intralumenal membranes. Proteins that regulate docking and fusion (Vac8p, the GTPase Ypt7p, its HOPS/Vps-C effector complex, the t-SNARE Vam3p, and protein phosphatase 1) accumulate at these vertices during docking. Their vertex enrichment requires *cis*-SNARE complex disassembly and is thus part of the normal fusion pathway.

Introduction

Organelle docking and fusion is catalyzed by a conserved set of chaperones (Sec18p/NSF, Sec17p/α-SNAP, and LMA1), integral membrane SNAREs which associate in *cis* (on the same membrane) or in *trans* (on docked organelle membranes), GTPases (Novick and Zerial, 1997), and Ca^{2+}-responsive proteins (Sudhof and Rizo, 1996; Burgoyne and Morgan, 1998). Little is known of the spatial relationships among these proteins, though proper spatial disposition may be essential for fusion.

We study organelle traffic through the homotypic fusion of yeast vacuoles (Wickner and Haas, 2000). This reaction occurs in three steps. "Priming" prepares vacuoles for attachment, or "docking," which leads to "fusion" and the complete mixing of lumenal contents. Priming is initiated by the Sec18p ATPase (Mayer et al., 1996), which disassembles *cis*-SNARE complexes of Vam3p, Vam7p, Vti1p, Ykt6p, and Nyv1p (Nichols et al., 1997; Ungermann et al., 1998a, 1999a) and releases Sec17p and the HOPS (homotypic fusion and vacuole protein sorting)/Vps-Class C complex. HOPS includes the Sec1p homolog Vps33p, the nucleotide exchange factor Vps39p, and Vps11, 16, 18, and 41p (Price et al., 2000b; Seals et al., 2000; Wurmser et al., 2000). After release from the *cis*-SNARE complex, HOPS activates Ypt7p (Ungermann et al., 2000; Wurmser et al., 2000) for the "tethering" stage of docking (Ungermann et al., 1998b). Tethering is essential for SNARE association in *trans* (Ungermann et al., 1998b). *trans*-SNARE complexes are essential for release of vacuolar Ca^{2+} (Peters and Mayer, 1998) but are then dispensable (Ungermann et al., 1998b, 1999b). Fusion requires a distinct cascade of protein actions. Released vacuolar Ca^{2+} activates calmodulin (Peters and Mayer, 1998), which associates with the V0 domain of the vacuolar ATPase and induces V0-V0 pairing in *trans* (Peters et al., 2001). Protein phosphatase 1 (Glc7p) triggers the last known stage of the fusion subreaction (Conradt et al., 1994; Mayer et al., 1996; Xu et al., 1998; Peters et al., 1999).

Since vacuoles are 1–3 μm in diameter, their surfaces are visible by light microscopy and amenable to analysis of spatial dynamics during docking and fusion. We now report that fusion does not occur at the "boundary" membrane where docked vacuoles touch, but rather at vertex rings around the disc of apposed boundary membrane. Proteins that are essential for docking and fusion (Ypt7p, Vps33p, Vps39p, Vam3p, Vac8p, and Glc7p) are enriched at vertices. Vertex ring fusion leaves boundary membrane in the lumen of the fused organelle.

Results

Many wild-type yeast have a few clustered vacuoles. Fusion of these vacuoles is readily triggered by activation of the MAP kinase pathway (Bone et al., 1998; Wang et al., 2001) by osmotic stress, caffeine, or heat. Time-lapse confocal microscopy of living cells with vacuoles labeled by both FM4-64 and GFP-tagged Vph1p, an integral membrane protein, reveals unexpected aspects of the fusion pathway (Figures 1A–1C; see Supplemental Movies 1–7, corresponding to these fusion events and others, at http://www.cell.com/cgi/content/full/108/3/357/DC1). Docked vacuoles have outside membrane, which is not in contact with other vacuoles, boundary membrane, which is apposed to a neighboring vacuole, and vertices, where boundary membranes or boundary and outside membranes meet.

Vacuole fusion in vivo begins with separation of the boundary membrane from the external membrane at vertex sites. This initial event of fusion can be monitored in three ways. First, a drop in fluorescence intensity is observed at vertex sites (Figure 1A, arrowheads). Second, the boundary membrane becomes mobile (resembling a flag in the wind) adjacent to the region of lowered fluorescence intensity. Third, the external membrane, which prior to fusion is sharply concave at the vertex site, relaxes to a flat or convex shape as its attachment to the boundary region is severed. Fusion terminates with release of the boundary membrane into the vacuole lumen, accompanied by an apparent increase in its Brownian motion and rounding of the external membrane. Boundary membrane that enters the lumen frequently fragments or vesiculates (Figures 1A–1C, see Supplemental Movies 1–7 at http://www.cell.com/cgi/content/full/108/3/357/DC1). The interval between the initiation of fusion and its completion by release of the

[1]For contact and other information, please see http://www.dartmouth.edu/~wickner

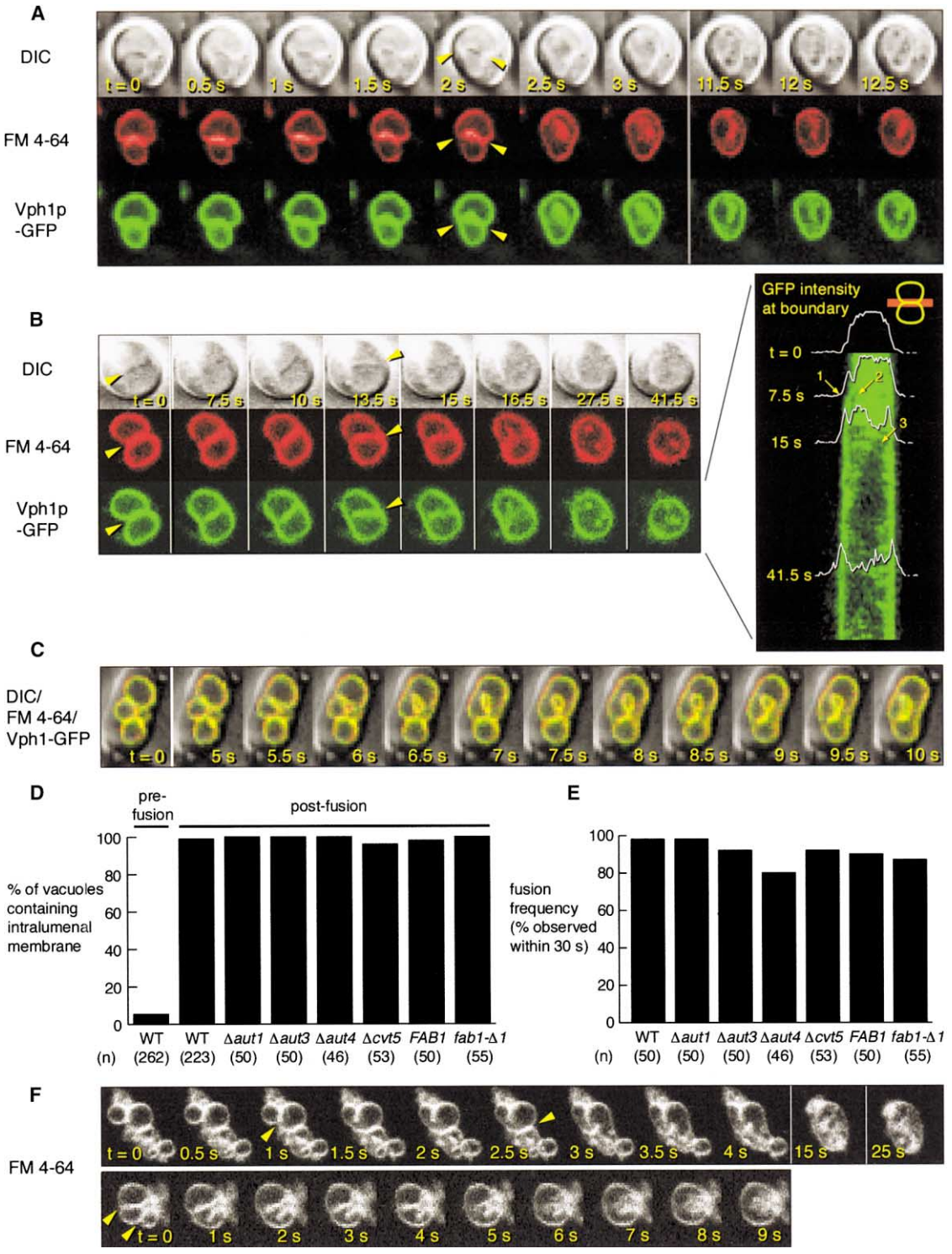

Figure 1. Vertex Ring Fusion

(A–C) Vacuole fusion initiates and completes at vertex sites. Cells expressing Vph1-GFP were grown to mid-log phase at 30°C with shaking in 10 ml YPD, 3 μM FM4-64 (Molecular Probes). Aliquots (250 μl) were sedimented, resuspended in 20 μl YPD, and applied to a flow cell (Wang et al., 2001). YPD with 24.0 mM caffeine was then perfused until nonadherent cells were cleared. Arrowheads denote sites where fusion is about to occur. Shown are frames from Supplemental Movies 1–3 at http://www.cell.com/cgi/content/full/108/3/357/DC1.

(D–E) Internal membranes arise from vacuole fusion in cells with defects in autophagy, CVT, or MVB transport. Cells were grown to mid-log at 30°C (the fab1-Δ1 mutant and its parent were grown at 24°C) in YPD with 3 μM FM4-64. Aliquots (250 μl) were centrifuged and the pellets were resuspended in 60 μl YPD or YPD + 24.0 mM caffeine and incubated 5 min at 23°C. Caffeine-treated cells containing apposed vacuoles were monitored for 30 s, and vacuole fusion and fusion-dependent internal-membrane formation frequencies were scored. Untreated control cells were examined and frequency of vacuolar internal membranes was determined (prefusion).

(F) Fusion initiates at vertices in vitro. Standard fusion reactions (Experimental Procedures) were incubated (27°C, 60–90 min), mounted in agarose with reaction fusion buffer, stained with FM 4-64, and subjected to time-lapse confocal microscopy. Arrowheads denote where fusion is about to occur. The top and bottom show frames from Supplemental Movies 8 and 9 at http://www.cell.com/cgi/content/full/108/3/357/DC1.

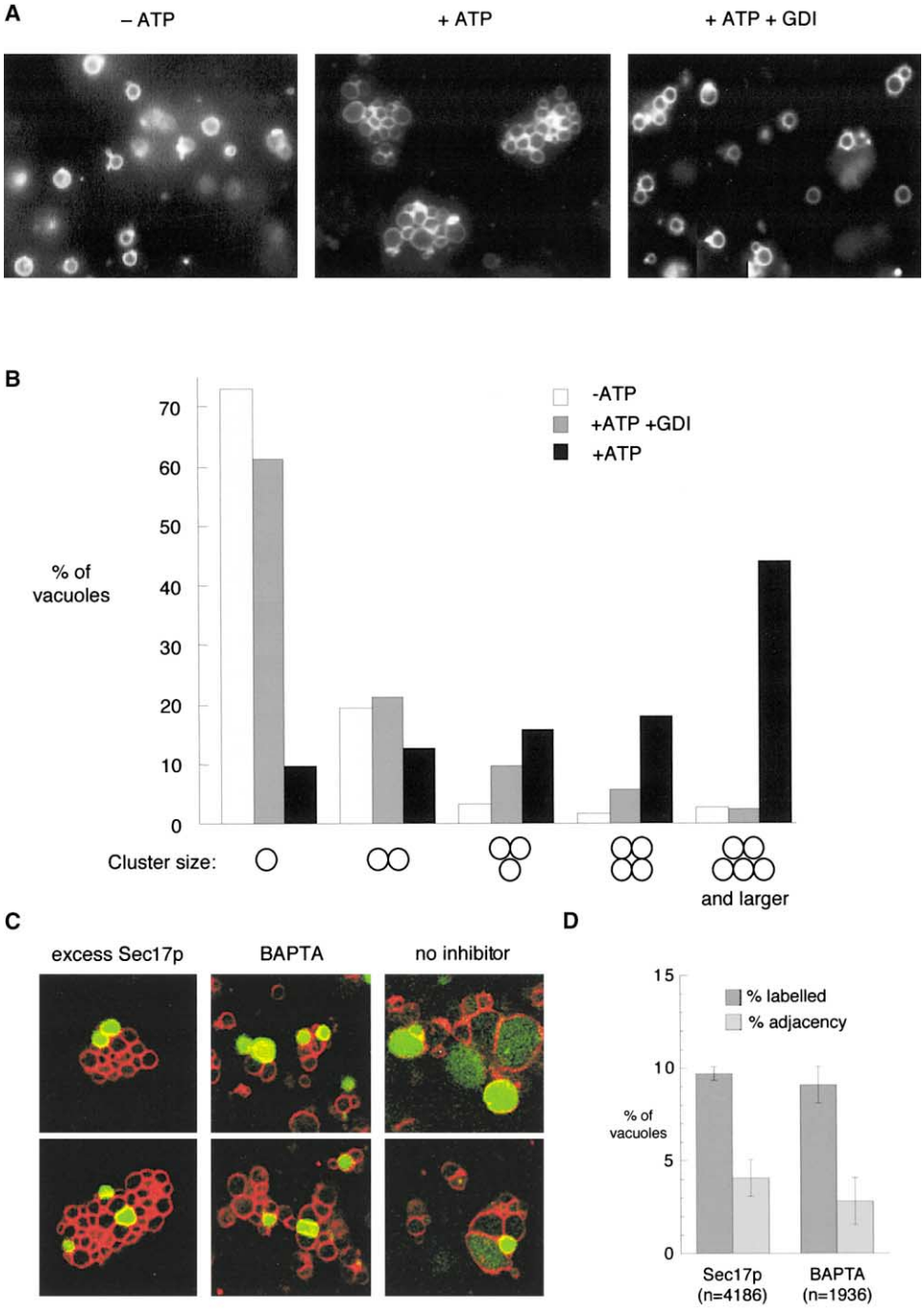

Figure 2. Authentic Docking

(A) Vacuole clustering is ATP-dependent and sensitive to Gdi1p. Purified vacuoles were used in a microscopic docking assay (Experimental Procedures) in the presence or absence of ATP and Gdi1p (300 μg/ml). Reactions (30 μl; 20 min, 25°C) were stopped by chilling on ice. Vacuoles were stained with FM4-64 (10 μM, 2 min, 0°C) and mixed with 150 μl of 0.8% low-melting agarose in PS buffer. Aliquots (15 μl) were transferred to prechilled slides and placed under a cover slip. After 10 min at 4°C, 50–100 random fields were observed by fluorescence microscopy in the rhodamine channel. A montage of representative clusters for each reaction are shown.

(B) The size of vacuole clusters reflects docking efficiency. Vacuole clusters were categorized as dimer, trimer, tetramer, or pentamer and larger. Approximately 500 vacuoles were counted for each reaction, and the percentage of vacuole clusters in each category was determined.

(C) Docked vacuoles lack large pores. Confocal micrographs of calcein-labeled (green) and FM4-64-counterstained (red) vacuoles, incubated with no inhibitor, excess Sec17p, or BAPTA.

(D) Reactions with a 1:10 ratio of calcein-labeled:unlabeled vacuoles and no inhibitor, excess Sec17p, or BAPTA were analyzed by confocal microscopy and scored for labeling (calcein-positive) and adjacency (calcein-positive and adjacent to another positive vacuole). Bars show means of three independent experiments with 95% confidence intervals.

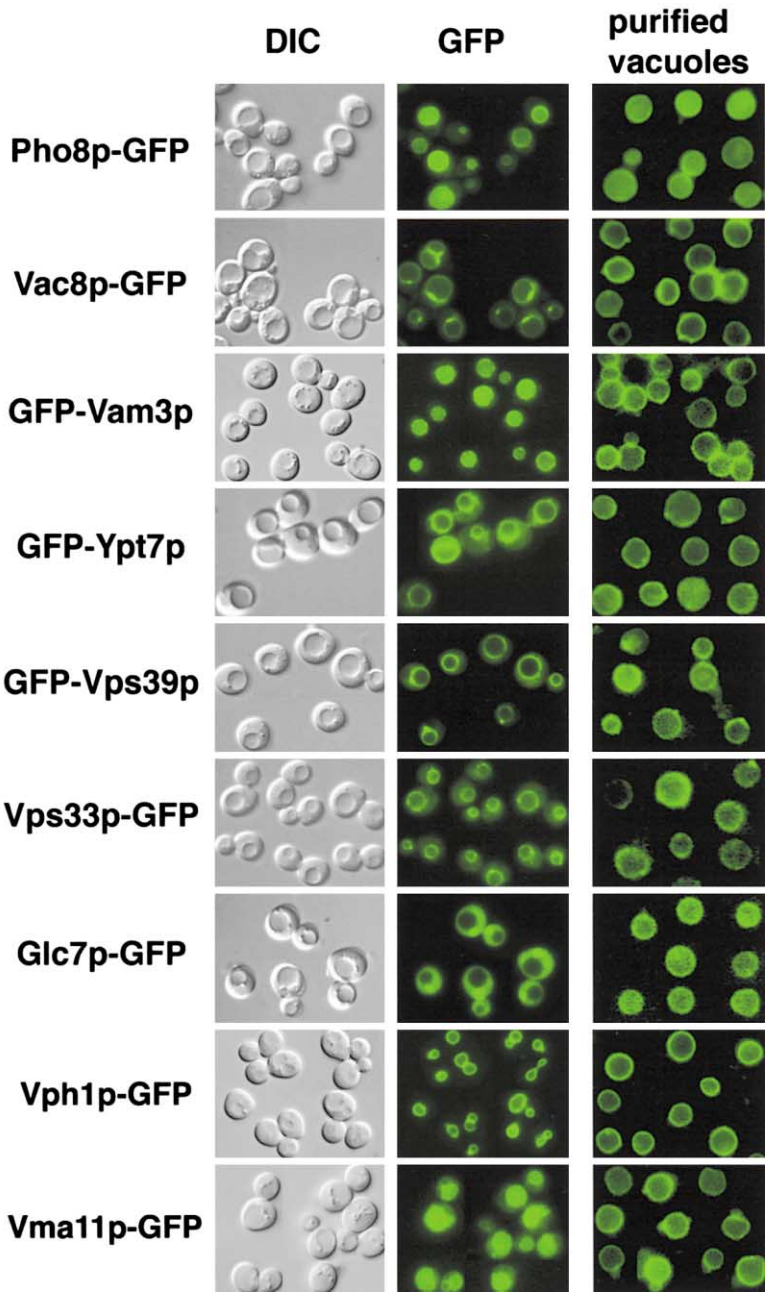

Figure 3. Vacuole Morphology

Cells with proteins tagged with GFP were grown in SD medium at 30°C to OD_{600} = 1–2, and then 1 ml of culture was centrifuged (10,000 × g, 2 min, 4°C), suspended in 1 ml of PBS (pH 7.5), collected as above, and suspended in 100 μl of SD medium. Cells were observed by Nomarski optics (DIC; 50 ms exposure) and by fluorescence microscopy in the FITC channel (1 s exposure). Vacuoles isolated from these strains were embedded in 0.8% low-melt agarose.

boundary membrane into the fused vacuolar lumen varies from <1 s (Figure 1A) to several seconds (Figure 1B). Quantitation of the fluorescence intensity along the boundary, from one vertex to the other, as a function of time (Figure 1B, right), shows a broadening of the profile of the fused vacuole membrane (Figure 1B, arrow 1) as the boundary membrane separates at the opposite vertex (arrow 2). Release at the opposite vertex occurs thereafter (arrow 3). In cells with clusters of several docked vacuoles, fusion often results in the formation of a single vacuole containing a large fragment of intralumenal membrane within a few seconds (Figure 1C). These observations indicate that vertices are functional sites of fusion initiation and propagation and that organelle-limiting membrane can be consumed through internalization rather than conserved during fusion.

Internal membrane formation was observed in 96% of fusion events (Figure 1D) but was seen in only 5% of docked vacuoles prior to fusion. Intralumenal membranes within endocytic organelles also arise through invagination and scission of the limiting membrane (Odorizzi et al., 1998), rather than as products of fusion events. For this reason we asked whether internal membranes would arise through fusion in mutants defective for the autophagy (aut), cytosol-to-vacuole (cvt), and multivesicular body (fab1) pathways. In each of these mutant strains, mobile intralumenal membranes were observed within the fused vacuoles (Figure 1D), and fusion occurred rapidly (Figure 1E). Thus, previously described membrane-invagination pathways cannot account for the accumulation of lumenal membranes during fusion.

Studies of in vitro fusion of purified vacuoles (Wickner and Haas, 2000) have established the stages of the reaction and identified responsible protein and lipid catalysts. Fusion of purified vacuoles that had docked in vitro also originates at vertices and yields lumenal membranes (Figure 1F, see Supplemental Movies 8 and 9 at http://www.cell.com/cgi/content/full/108/3/357/DC1). Multiple fusion events can occur within seconds (Figure 1F, arrows), with kinetics that are comparable to those seen in vivo (Figures 1A–1E).

Docked Vacuole Clusters with GFP-Tagged Proteins

Since fusion occurs at vertices of docked vacuoles, the proteins that catalyze this reaction may be enriched at vertex sites. To test this, we need authentic docking clusters and visible fluorescent tags on individual proteins. As reported (Mayer and Wickner, 1997), primed vacuoles form large docked clusters well before fusion (Figure 2A). Formation of clusters of five or more vacuoles (Figure 2B) requires ATP and is sensitive to Gdi1p, which extracts Ypt7p and blocks tethering/docking (Haas et al., 1995; Mayer and Wickner, 1997). To determine whether these docked vacuoles have detectable fusion pores, vacuoles were loaded with calcein, a polyanionic fluorophore of 623 Da. Calcein-loaded vacuoles were mixed with unlabeled vacuoles at a ratio of 1:10 and counterstained with FM4-64. Standard fusion incubation yields large vacuoles with lumenal calcein (Figure 2C). We asked whether detectable pores form between vacuoles after they first associate (tethering) but before Ca^{2+}-triggered fusion. Excess Sec17p blocks fusion at an early stage. It allows priming but recaptures SNAREs into a *cis*-complex, blocking all steps after tethering (Wang et al., 2000). BAPTA blocks a late Ca^{2+}-dependant step, downstream of *trans*-SNARE pairing (Peters and Mayer, 1998; Ungermann et al., 1999b). The diameters of vacuoles incubated with excess Sec17p or BAPTA remained similar to freshly isolated vacuoles (Figure 2C). Calcein transfer between docked vacuoles would have increased both the number of labeled vacuoles and the fraction that are adjacent to other labeled vacuoles ("adjacency" is the percentage of vacuoles which are both calcein-labeled and share boundary membrane with other labeled vacuoles). Neither labeling nor adjacency indices increased in the presence of BAPTA as compared to samples with excess Sec17p (Figure 2D). Thus, though small or transient fusion pores may form during docking, the transfer of small (623 Da) as well as large aqueous probes (e.g., Pep4p in our standard assay) is not a simple consequence of docking but occurs only at the last kinetically distinguishable stage of vacuole fusion.

Armed with the ability to generate authentic docking clusters in vitro, we then GFP tagged the vacuolar t-SNARE (Vam3p), HOPS complex subunits (Vps39p, Vps33p), a small G protein (Ypt7p), protein phosphatase 1 (Glc7p), V0 subunits Vma11p and Vph1p, and Vac8p, a protein involved in vacuole inheritance and fusion (Pan and Goldfarb, 1998; Wang et al., 2001; Veit et al., 2001). Vacuolar alkaline phosphatase (Pho8p) provided a control, since it has no direct role in the fusion pathway. Each protein was expressed under its own promoter. Each of these strains, expressing a GFP-tagged protein in place of the wild-type, has normal vacuole morphology (Figure 3), and each fusion protein is evenly distributed on the surface of isolated vacuoles. Glc7p is largely cytosolic.

Table 1. Relative Abundance Levels of GFP-Tagged Proteins on Vacuole Membranes and Their Enrichment at Interfaces of Docked Vacuoles

GFP-Tagged Proteins		Relative Abundance	Enrichment at Docking Site
Vacuolar marker	Pho8p	N.D.	−
Vacuole inheritance	Vac8p	150	+
t-SNARE	Vam3p	40	+
HOPS complex	Vps39p	33.3	+
	Vps33p	20	+
GTPase	Ypt7p	400	+
Protein phosphatase I	Glc7p	67	+
Vacuolar ATPase	Vph1p	200	−
	Vma11p	50	−

The abundance of GFP-tagged proteins, expressed under their native promoters, was compared to that on wild-type vacuoles by immunoblot and was unaltered (see Supplemental Figure S1A at http://www.cell.com/cgi/content/full/108/3/357/DC1). As each protein was tagged with the same GFP module, we could compare their relative abundance on vacuole membranes by immunoblot (Table 1; see Supplemental Figure S1B). The relative abundance of these proteins ranges from Ypt7p (400 relative units) to Vam3p (40) and Vps33p (20).

We also examined the vacuole-targeting efficiency of these proteins in wild-type cells or after fusion with GFP (see Supplemental Figure S2 at http://www.cell.com/cgi/content/full/108/3/357/DC1), and we found that the wild-type (see Supplemental Figure S2A) and GFP-tagged (see Supplemental Figure S2B) proteins are targeted to vacuoles with similar efficiencies. The functionality of the GFP-tagged proteins was examined by the in vitro homotypic vacuole fusion assay. The loss of function of any of these proteins blocks vacuole fusion (Haas et al., 1995; Nichols et al., 1997; Ungermann and Wickner, 1998; Peters and Mayer, 1998; Ungermann et al., 1999a; Peters et al., 1999; Price et al., 2000a). Vacuoles with each of the GFP-tagged proteins have normal fusion activity (see Supplemental Figure S3) and are thus functionally intact.

Vertex Enrichment of Fusion Proteins

Our microscopic assay of docking, combined with GFP-tagging, allows study of protein enrichment at docking sites. In docked vacuole clusters, proteins may be evenly distributed over the vacuole surface or may be enriched at outside edges, at the boundary midpoints (the center of where the membranes of two docked vacuoles are apposed), or at vertices, where outside edge meets border or where multiple boundary regions meet (Figure 4A). Due to the geometry of docked vacuoles, larger amounts of membrane are present at the borders between docked vacuoles and at the vertices than at the outside edges of vacuole clusters. We therefore used ratiometric fluorescence microscopy to study the enrichment of GFP-tagged proteins with respect to the lipophilic styryl dye FM4-64, providing a quantitative measure of local changes in GFP concentration per unit membrane.

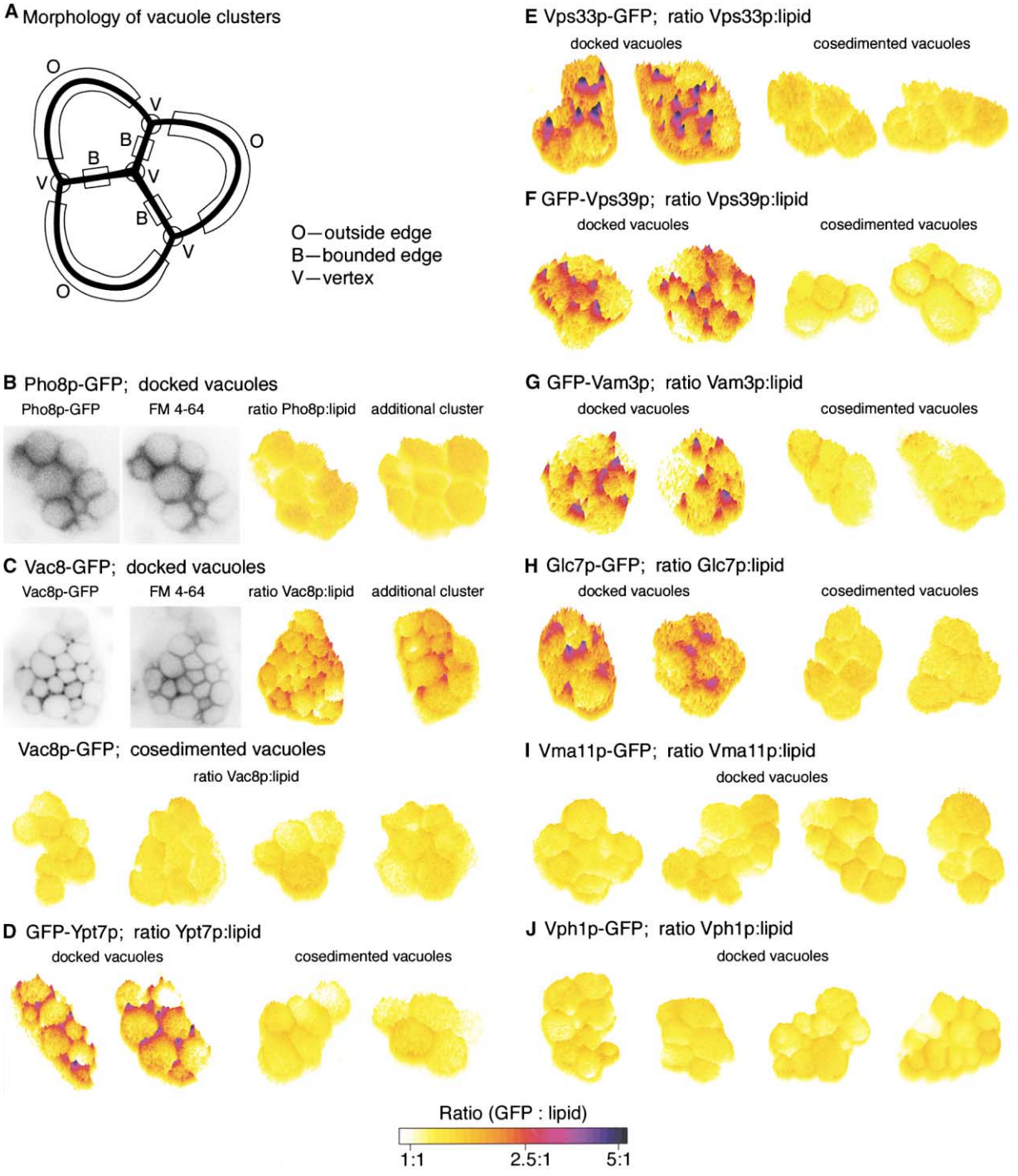

Figure 4. Protein Distributions on Docked Vacuoles

(A) The membrane regions of docked vacuoles are outside, boundary, and vertices.

(B) The FM4-64 and GFP channel images of a docked cluster of Pho8p-GFP vacuoles, and their ratio after subtracting background (Experimental Procedures).

(C–J) Vacuoles were either docked or clustered by cosedimentation without docking incubation, as indicated, and analyzed for the ratio of GFP to FM4-64 fluorescence as described in Experimental Procedures.

Vacuoles bearing the various GFP-tagged proteins were primed and docked, stained, and observed by fluorescence microscopy. To determine whether observed distributions of GFP-tagged proteins were specific to authentic docking, control vacuole clusters were prepared by sedimentation of unprimed vacuoles. Sedimentation causes vacuole clustering, which cannot bypass the normal Ypt7p-, HOPS-, and SNARE-dependent mechanisms of the authentic fusion pathway.

To establish the utility of the ratiometric assay, we

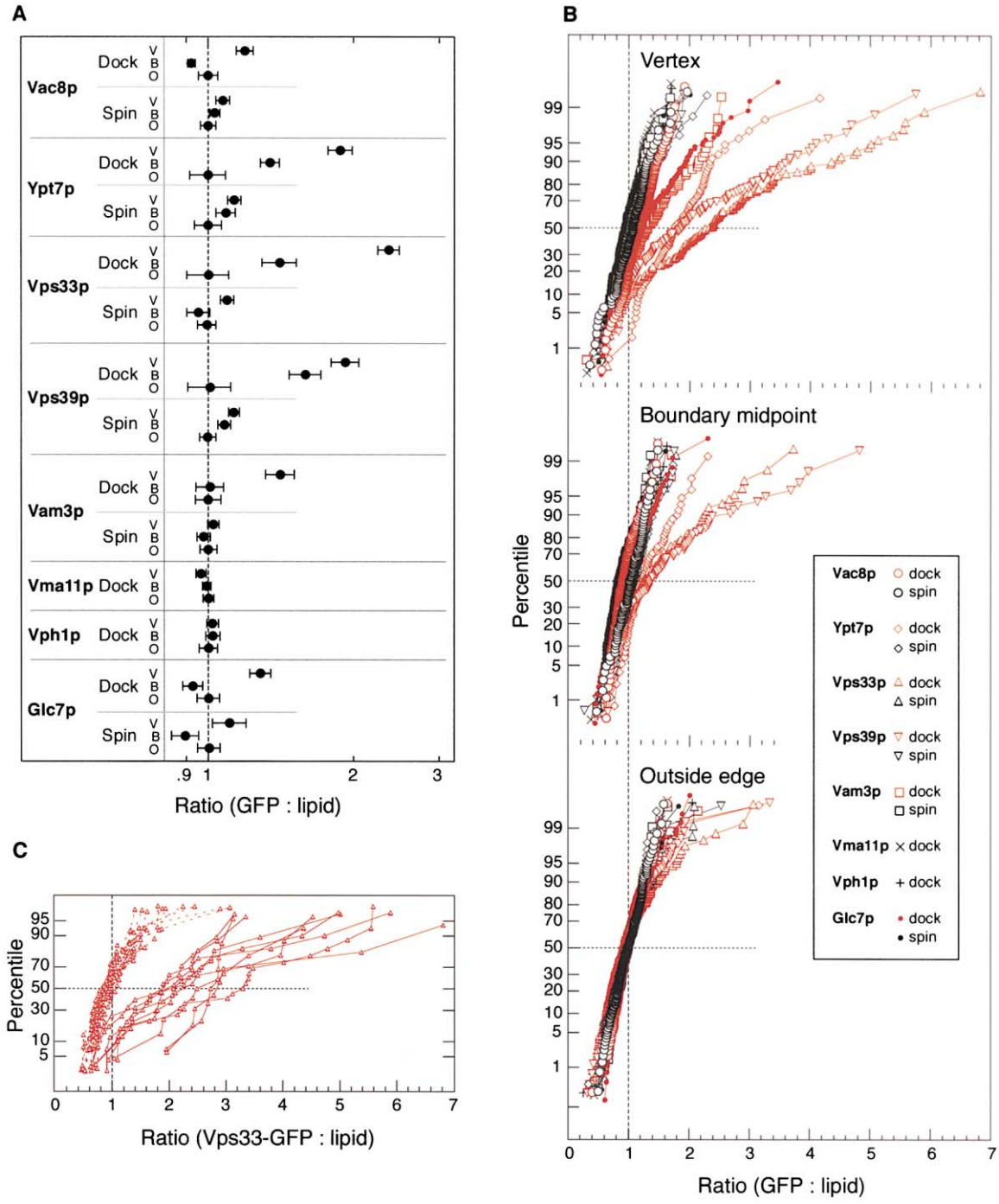

Figure 5. Morphometric Analysis of Protein Localization

(A) Mean ratios. Each bar shows mean ratio ± 95% confidence intervals. Vacuoles were docked or cosedimented (spin). Morphological classes are (V)ertex, (B)oundary midpoint, and (O)utside edge.

(B) Cumulative distribution plots show the range of values obtained for each location. The intersection of each data series with the 50th percentile line indicates the median value. For each treatment, an average of 408 individual ratio measurements on 10–15 vacuole clusters were obtained from at least two independent experiments. More than 700 individual ratio measurements are summarized in this figure.

(C) Cumulative distribution plots of data for individual clusters bearing Vps33-GFP. Each line connects measurements for a single cluster of vacuoles. Solid lines show vertex measurements; dashed lines show outside edge measurements.

studied GFP-tagged Vac8p, known to be enriched at vacuole:vacuole junctions in vivo (Pan and Goldfarb, 1998), and Pho8p, a vacuolar membrane protein that is not required for membrane fusion. Pho8-GFP was distributed homogenously on docked vacuoles (Figure 4B). In contrast, Vac8-GFP concentrates at vacuole-vacuole junctions (Figure 4C) with the largest accumulations of Vac8-GFP found in punctate structures at the

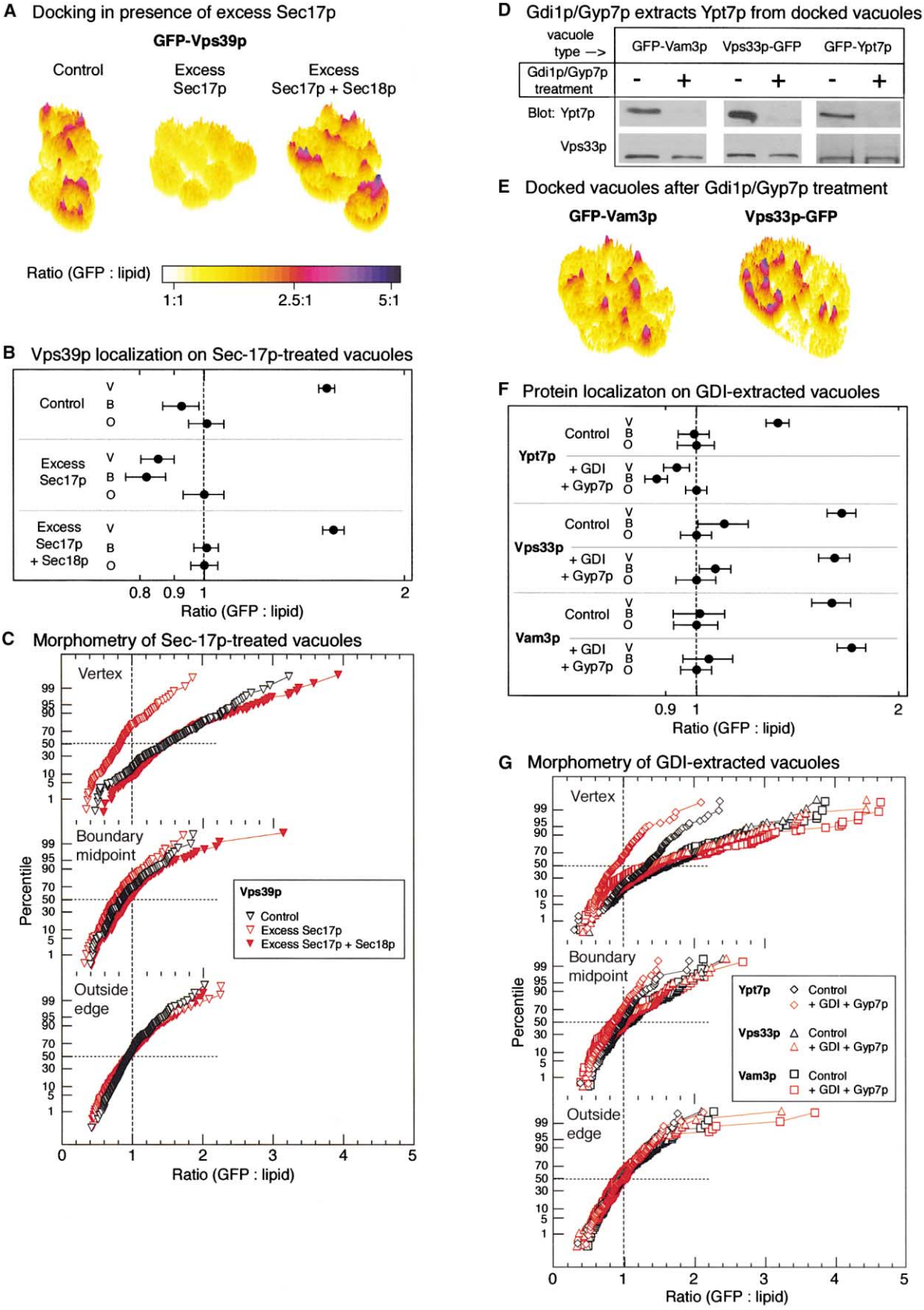
A Docking in presence of excess Sec17p
GFP-Vps39p
Control
Excess Sec17p
Excess Sec17p + Sec18p
Ratio (GFP : lipid)
1:1
2.5:1
5:1
B Vps39p localization on Sec-17p-treated vacuoles
Control
Excess Sec17p
Excess Sec17p + Sec18p
V
B
O
0.8 0.9 1 2
Ratio (GFP : lipid)
C Morphometry of Sec-17p-treated vacuoles
Vertex
Boundary midpoint
Outside edge
Percentile
Vps39p
Control
Excess Sec17p
Excess Sec17p + Sec18p
0 1 2 3 4 5
Ratio (GFP : lipid)
D Gdi1p/Gyp7p extracts Ypt7p from docked vacuoles
vacuole type —>
GFP-Vam3p
Vps33p-GFP
GFP-Ypt7p
Gdi1p/Gyp7p treatment
- + - + - +
Blot: Ypt7p
Vps33p
E Docked vacuoles after Gdi1p/Gyp7p treatment
GFP-Vam3p
Vps33p-GFP
F Protein localizaton on GDI-extracted vacuoles
Ypt7p
Vps33p
Vam3p
Control
+ GDI + Gyp7p
V
B
O
0.9 1 2
Ratio (GFP : lipid)
G Morphometry of GDI-extracted vacuoles
Vertex
Boundary midpoint
Outside edge
Percentile
Ypt7p
Vps33p
Vam3p
Control
+ GDI + Gyp7p
0 1 2 3 4 5
Ratio (GFP : lipid)

vertices. Morphometric analysis (Figure 5) shows that the enrichment is significant. Vac8p was not enriched at vertices in cosedimented clusters (Figure 4C), indicating that Vac8-GFP accumulation occurs during docking but not as a nonspecific consequence of vacuole:vacuole contact.

We next examined the localization of those proteins, which are established as participating directly in each stage of the vacuole fusion reaction. GFP-tagged Ypt7p (Figure 4D), the vacuole Rab/Ypt GTPase, and two subunits of its HOPS effector complex, Vps33p and Vps39p (Figures 4E and 4F), were strongly enriched at the vertices of vacuoles, that were authentically docked but not at junctions between vacuoles clustered by sedimentation. Vam3p-GFP also accumulated at vertices of docked vacuoles but not of vacuoles clustered by sedimentation (Figure 4G). Protein phosphatase 1 (Glc7p) triggers the fusion of docked vacuoles and is the last known catalyst in the vacuole fusion cascade. Glc7p-GFP localizes to the vertices of docked vacuoles but is not enriched at vertices when vacuoles are clustered by sedimentation (Figure 4H). In contrast, the V0 subunits Vma11p and Vph1p, tagged with GFP, are not detectably enriched at boundaries or vertices of docked vacuoles (Figures 4I and 4J). Since Vph1p is a 100 kDa polypeptide, the vertex enrichment seen for other proteins does not arise from an exclusion of bulky proteins from the boundary regions. Taken together (Table 1), protein accumulation at docking junction vertices is a regulated and selective process.

Localization data was subjected to morphometric analysis (Figure 5). In docked vacuoles, the enrichment of Vac8, Ypt7p, Vps33p, Vps39p, Vam3p, and Glc7p at the vertices (V) is highly significant (Figure 5A) and different from the corresponding outside edge values ($p < 0.005$ for Glc7p, $p < 0.0001$ for the others). Each mean ratio of GFP-tagged protein to lipid is shown with its 95% confidence interval. Enrichments are readily visualized with cumulative distribution plots (Figure 5B). In such plots, each of the ratio values is presented as a data point; as a cohort, they form a curve. Curves are shown for each GFP-labeled protein, each position within the vacuole cluster (outside, boundary midpoint, or vertex), and each means of vacuole clustering (docking or cosedimentation). The ratios are ordered and plotted versus the percentile rank of the values. All of the data cohorts for outside edges span a narrow range of ratios, independent of which protein was GFP-tagged or whether the vacuoles were docked or cosedimented (Figure 5B, bottom). In contrast, the boundary midpoints of docked vacuoles show some enrichment of Ypt7p, Vps33p, and Vps39p (Figure 5B, middle). The most striking quantitative enrichment is seen at the vertices of docked vacuoles (Figure 5B, top) for Vac8p (red open circles), Glc7p (red filled circles), Ypt7p (red diamonds), Vps33p (red triangles), Vps39p (red inverted triangles), and Vam3p (red squares). Almost the entire range of enrichment values of these proteins at the vertices of docked vacuoles is significantly shifted from that seen at outside edges (bottom) or at the vertices of vacuoles clustered by sedimentation (top, corresponding black symbols). The enrichment of proteins such as Vps33p was not just seen at the vertices of a few docked vacuole clusters. Rather, every cluster examined showed a comparable range of vertex enrichment values (Figure 5C, solid lines), and these were well resolved from the values at outside edges (dotted lines). The greater enrichment at vertices of Vps33p and Vps39p relative to Ypt7p may reflect that Ypt7p has >10 times the molar abundance as these HOPS subunits on vacuoles. Even if stoichiometric complexes were to assemble at vertices between HOPS and Ypt7p, the greater molar abundance of Ypt7p might account for its lower ratio of enrichment.

Two tests were performed to determine whether vertex enrichment of proteins is part of the normal vacuole fusion pathway. Excess Sec17p allows priming, but the SNAREs are recaptured into a *cis*-complex (Wang et al., 2000). Vacuole tethering in the presence of excess Sec17p still requires Ypt7p; clusters of five or more vacuoles accounted for 60% of vacuoles in standard incubations and 67% in the presence of excess Sec17p, but only 9% in the presence of both excess Sec17p and added Gdi1p. However, tethered vacuole clusters that are formed in the presence of excess Sec17p do not show protein enrichment at contact domains (Figures 6A–6C). The block by excess Sec17p is overcome as *cis*-SNARE complexes are disassembled by excess Sec18p (Wang et al., 2000), and vertex enrichment is restored as well (Figures 6A–6C). Since this disassembly of *cis*-SNARE complexes by Sec18p is essential for vertex protein enrichment, this enrichment lies on the authentic fusion pathway.

The need for Ypt7p during a transient reaction segment, after priming and before *trans*-SNARE pairing, provided a second test of whether vertex enrichment is part of the normal docking pathway. Ypt7p is abundant

Figure 6. Vertex Enrichment Is on the Pathway to Fusion

(A) Effects of Sec17/18 action on vertex enrichment. Vacuoles with GFP-Vps39p were used for in vitro docking. Excess Sec17p (100 ng/μl) and excess Sec18p (80 ng/μl) were added at the beginning of the reaction where indicated. Ratiometric images of representative clusters are shown.

(B and C) Quantitative analysis, as in Figure 4, of multiple vacuole clusters (>500 ratio measurements for each reaction) for outside edge, boundary midpoint, and vertices.

(D–G) Stable vertex localization of Vps33p and Vam3p after Ypt7p extraction from docked vacuoles. Vacuoles (20 μg) from strains expressing GFP-Vam3p, Vps33-GFP, and Ypt7-GFP were used for in vitro docking. After 20 min at 27°C, Gdi1p (100 μg/ml) and Gyp7p (30 μg/ml) were added or, for controls, an equal volume of buffer (10 mM Pipes/KOH [pH 6.8], 200 mM sorbitol). After 30 min, 5 μg of vacuoles were analyzed by fluorescence microscopy while the rest were collected by centrifugation (10,000 rpm, 5 min, microfuge, 4°C).

(D) Vacuole pellets were analyzed by immunoblot.

(E) Ratiometric images of representative clusters of Vps33-GFP and Vam3-GFP after Ypt7p extraction.

(F and G) Quantitative analysis, as in Figure 5, of multiple vacuole clusters (2,773 individual ratio measurements) for each of the three vacuole preparations, with or without extraction of Ypt7p, for outside edge, boundary midpoint, and vertices.

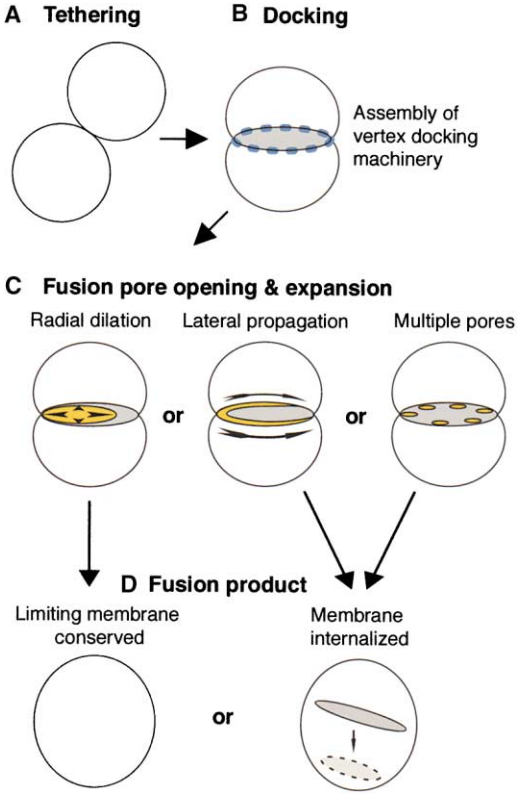

Figure 7. Working Model

(Table 1), enriched at the vertices of docked vacuoles (Figures 4 and 5), and essential to initiate docking (Figure 2; Mayer and Wickner, 1997), yet is no longer needed after docking is complete (Eitzen et al., 2000). We asked whether the HOPS subunit Vps33p and the t-SNARE Vam3p would remain at the vertices of docked vacuoles when Ypt7p was extracted by incubation with recombinant Gyp7p, its GTPase activating protein, and Gdi1p. This extraction is efficient and does not interfere with subsequent fusion (Eitzen et al., 2000). Vacuoles bearing GFP-tagged Ypt7p, Vps33p, or Vam3p were allowed to dock, then incubated with buffer or with Gdi1p and Gyp7p, reisolated, and assayed by immunoblot (Figure 6D); 90%–93% of the Ypt7p was extracted, with more efficient extraction from the vertices than from the boundary and edge regions (Figure 6G, red versus black diamonds; $p < 0.0001$). Most of the Vps33p remained vacuole bound (Figure 6D). Strikingly, the localization and vertex enrichment of Vps33p and Vam3p were not significantly altered by extraction of Ypt7p from docked vacuoles ($p > 0.8$, $p > 0.3$, respectively; Figures 6E–6G). Though Ypt7p and HOPS cooperate to initiate docking, Ypt7p is not needed to maintain the vertex protein assembly once formed. HOPS, a peripheral membrane complex that binds Ypt7p (Price et al., 2000b), must then associate with other components such as Vam3p, which act downstream of Ypt7p.

Discussion

Vertex ring fusion has two spatial hallmarks, the release of boundary membrane from the vertices and the appearance of this released membrane within the lumen of the fused organelle. In this regard, vertex fusion is fundamentally distinct (Figure 7) from radial pore expansion models of fusion. In the latter models, fusion that is initiated at any point on the boundary membrane would convert all the boundary membrane to outside membrane. In contrast, boundary membrane becomes entrapped in the fused organelle by vertex ring fusion, though the fate of entrapped membrane is unknown. Intralumenal membrane may fuse back to the outside membrane or may be degraded by hydrolytic enzymes (Odorizzi et al., 1998). The generation of intralumenal membrane during fusion might serve physiological functions such as regulating the vacuole surface-to-volume ratio.

How general is vertex ring fusion? Intralumenal membranes are present in autophagosomes, CVT vesicles, multivesicular bodies, and major histocompatibility class II loading compartments (de Duve and Wattiaux, 1966; Hirsch et al., 1968; Odorizzi et al., 1998; Denzer et al., 2000). Most intralumenal membranes are thought to be produced by the invagination and scission of limiting membranes. However, an additional possibility, that intralumenal membranes arise as products of membrane fusion, was proposed more than 35 years ago (Miller and Palade, 1964; de Duve and Wattiaux, 1966) based on morphological observations. Our experiments show that this mechanism operates in vivo. In experiments using erythrocytes as a model for membrane fusion, Chernomordik and Sowers (1991) observed strings of fusion pores and "considerable internal vesicle membrane fragments." Finally, the rosettes of membrane-intercalated particles seen at exocytic sites in paramecium (Olbricht et al., 1984) may be analogs of the vertex protein complexes reported here. This idea is reinforced by recent findings that NSF action is needed to establish fusion site rosette formation (J. Cohen, personal communication), just as Sec17/18P action is required for vacuole vertex ring formation (Figures 6A–6C).

Rabs, SNAREs, and Rab effectors, which concentrate at the vertices, catalyze reactions, that lead to fusion of vacuoles and other organelles. However, we do not know the complete complement of proteins and lipids that are enriched at vertex rings or the mechanism of the terminal, bilayer-mixing steps of the fusion reaction. Additional proteins such as Rho GTPases (Eitzen et al., 2000) may be enriched at vertices and play crucial roles. Though the vertex enrichment of selected proteins requires Sec17/18p action and is thus on the normal fusion pathway, the mechanism of enrichment is unknown. It might entail *trans*-SNARE complex formation, *trans*-V0 complex formation, lipid microdomains, remodeling organelle bound actin, or assembly of a proteinaceous scaffold. It need not represent stoichiometric associations among the vertex-enriched components. Finally, it is unclear how SNAREs, V0 domains, and other factors cooperate to catalyze the actual bilayer mixing step. A deeper understanding of the relation between vertex ring enrichment of selected proteins and vertex ring fusion will have to include identifying those components which specifically either localize proteins to vertices or catalyze fusion.

Our studies suggest a speculative model of vacuole docking and fusion (Figure 7). Priming disassembles the *cis*-SNARE complex (Ungermann et al., 1998a, 1999a)

and allows HOPS (Seals et al., 2000) to associate with Ypt7p, catalyzing nucleotide exchange to its GTP bound state (Wurmser et al., 2000) and promoting tethering (Figure 7A). Vps33p and Vps39p (HOPS), Ypt7p, Vam3p, Vac8, and protein phosphatase 1 (Glc7p) accumulate at the vertices of docked vacuoles (Figure 7B). Our studies do not specify whether these proteins accumulate at vertices concurrently or in a defined order. While the factors responsible for localizing docking and fusion catalysts to vertices are unknown, the Cdc42p and Rho1p GTPases, which act after Ypt7p during vacuole docking (Eitzen et al., 2000) and control spatial aspects of fusion in other systems (Hall, 1998; Guo et al., 2001), are attractive candidates. Ypt7p might initiate vertex clustering, as it has a central role in tethering (Ungermann et al., 1998b). However, Ypt7p is not needed to maintain docked vacuole structure or to keep either HOPS or Vam3p at vertices once these structures are established (Figures 6D–6G). HOPS, having associated with Ypt7p, then transfers to other vertex components, possibly via an affinity of its Vps33p (Sec1p-homolog) subunit for the Vam3p t-SNARE (Price et al., 2000b; Sato et al., 2000; Dublova et al., 2001). The movement of large complexes such as HOPS to the vertex (Figure 7B) may permit the membrane lipid bilayers to attain close apposition, though large proteins such as Vph1p remain in the boundary domain. It is possible that the strain of curvature, introduced into the bilayer at vertices, may promote lipid transition to a fusion state. Fusion around a vertex ring (Figure 7C, middle and right) is triggered by protein phosphatase 1 (Conradt et al., 1994; Peters et al., 2001). Completion of fusion at sites around the ring and merging of multiple adjacent fusion pores, or propagation of a fusion signal around a ring of sites, causes internalization of boundary membrane (Figure 7D, right) and content mixing. In contrast, the classic fusion model of the radial expansion of a single fusion pore (Figures 7C and 7D, left) would not result in the internalization of boundary membrane.

Experimental Procedures

S. cerevisiae strains used in this study were BJ 3505 (*MAT*α *pep4::HIS3 prb1-1.6R HIS3 lys2-208 trp1-101 ura3-52 gal2 can*), BJ 2168 (*MAT*α *leu2-3,112 trp1-101 ura3-52 prb1-1122 pep4-3 pcr1-407*), DKY6281 (*MAT*α *leu2-3 leu2-112 ura3-52 his3-200 trp1-901 lys2-801 suc2-9 pho8::TRP1*), and SEY6210 (*MAT*α *leu2-3 leu2-112 ura3-52 his3-200 trp1-901 lys2-801 suc2-9*). D. Koshland generously provided *fab*1-Δ1 and its isogenic *FAB*1 parent (Yamamoto et al., 1995); *aut1*Δ, *aut3*Δ, *aut4*Δ, *cvt5*Δ, and the isogenic parent BY4742 were obtained from Research Genetics, Inc. The genotypes of strains expressing GFP-tagged proteins are summarized in Supplemental Table S1 at http://www.cell.com/cgi/content/full/108/3/357/DC1, and the oligonucleotides used in their construction are listed in Supplemental Table S2; the GFP used was the "Superglow" variant of Kahana and Silver (1998). For the C-terminal tagging of Pho8p, Vac8p, Nyv1p, Vps33p, and Glc7p, the GFP module was fused in frame to the 3′ end of the chromosomal copy of the gene by homologous recombination (Longtine et al., 1998). For N-terminal tagging of Vam3p, Vam6p, and Ypt7p, the chromosomal copy of each gene was first disrupted (Longtine et al., 1998). Integrating vectors (Supplemental Table S3) containing the GFP module fused in-frame to the 5′ end of the gene (or, for Vam3, two tandem in-frame GFP modules), flanked by its native promoter and part of the downstream region, were transformed into the deletion strain. Integrants were confirmed by PCR.

Vacuole Isolation and In Vitro Fusion Assay

Vacuoles were isolated (Haas et al., 1994) from GFP derivative strains. Standard reactions containing 3 μg each of vacuoles with GFP-tagged protein and BJ3505 or DKY6281 vacuoles and reaction buffer (10 mM Pipes/KOH [pH 6.8], 200 mM sorbitol, 120 mM KCl, 0.5 mM $MgCl_2$, 1 mM ATP, 7.5 μM pefablock SC, 7.5 ng/ml leupeptin, 3.75 μM *o*-phenanthroline, 37.5 ng/ml pepstatin A, 20 mM creatine phosphate, and 35 U/ml creatine kinase) were incubated (27°C, 90 min). Alkaline phosphatase activity was measured (Haas et al., 1994). One unit of alkaline phosphatase activity is 1 μmol of *p*-nitrophenol released/min/μg vacuoles.

In Vitro Microscopic Docking Assay

The docking assay was according to Mayer and Wickner (1997) with minor modification. Reactions (30 μl) contained 5 μg of GFP-tagged vacuoles, reaction buffer (10 mM Pipes/KOH [pH 6.8], 200 mM sorbitol, 40 mM KCl, 0.1 mM $MgCl_2$, 0.3 mM ATP, 7.5 μM pefablock SC, 7.5 ng/ml leupeptin, 3.75 μM *o*-phenanthroline, 37.5 ng/ml pepstatin A, 6 mM creatine phosphate, and 10 U/ml creatine kinase), and 500 μg/ml cytosol (Conradt et al., 1992). After incubation (27°C, 20 min), samples were chilled on ice, stained with 10 μM FM4-64 for 2 min, and then mixed with 150 μl of 0.8% low-melt agarose in PS buffer (10 mM Pipes/KOH [pH 6.8], 200 mM sorbitol). Aliquots (15 μl) were immediately transferred to prechilled slides and cover slips. After 10 min at 4°C, samples were observed by fluorescence microscopy. Images were acquired of 50–100 random fields.

GFP Fluorescence Microscopy and Image Processing

Images were acquired with a Zeiss Axioplan 2 fluorescence microscope equipped with a 100/1.4 NA Plan Apochromat objective, AttoArc halogen light source, and Hammamatsu Orca 2 camera with OpenLab software. The camera was operated at the normal gain setting with 2 × 2 pixel binning. FM4-64 fluorescence was always significantly brighter than GFP fluorescence. To compensate, the FM4-64 channel was used to locate fields and focus and was photographed first. The filters used to observe GFP fluorescence minimized optical bleedthrough from FM4-64 emission (excitation bandpass [nm] 450–490; 495 dicroic; emission bandpass 500–550; Chroma Technologies, Brattleboro, Vermont). Nevertheless, detectable crosstalk was noted. For this reason the FM4-64 dye was photobleached for 30–60 s prior to GFP data acquisition. Image processing and quantitative analysis employed Image/J v1.21e (http://rsb.info.nih.gov/ij/) running under Macintosh Runtime for Java v2.2.4 or MacOS X. Surface plots for ratio data were generated with NIH Image v1.62 (http://rsb.info.nih.gov/nih-image/). For ratio images, 14-bit images stored in 16-bit TIFF format were cropped to the region of interest (ROI), typically one cluster of vacuoles. Background was defined as the local minimum value of the cropped image and was subtracted. The local minimum value in cropped images was typically ~2 rmsd below the modal pixel value of the nonvacuole area in the uncropped image. Other methods of background subtraction, such as subtraction of images of no-vacuole samples, yielded similar results but suffered from significant variability due to temporal instability of the light source. Background-corrected images were thresholded by setting pixels with low values to zero, and were then converted to 32-bit (floating point) format to retain decimal precision without scaling of the data. Ratio images were generated using the pixel math: log G − log F = log R, where G is the value of a GFP pixel, F is the value of the corresponding FM4-64 pixel, and R is the ratio of these values. No attempt was made to compensate for the point-spread functions of the optics (e.g., iterative deconvolution); thus, the calculated ratios represent lower-bound indices of GFP accumulation at resolution-limited sites. Relative ratios are depicted in the figures by normalizing the visual contrast scales to a 5-fold range of ratio values on a logarithmic scale. The resulting range-calibrated images were converted to 8-bit format for production of surface plots and layout.

For morphometric analysis, images were background-subtracted, and then the measurement tool in Image/J was used to determine the GFP:lipid ratios between the maximum pixel values within manually placed circular 4–8 pixel diameter ROIs. This procedure compensated for slight misalignments between GFP/FM4-64 image pairs. Ratio measurements were pooled into three morphological

classes: outside edge, boundary midpoint, and vertex (see Figure 3A). Every vertex within a vacuole cluster was scored, and each outside edge was scored at multiple locations to increase sampling density. For each treatment, images of 10–15 clusters obtained from at least two independent experiments were scored. For each treatment, ratios were measured at an average of 423 individual sites. To facilitate comparisons between different treatments, all the ratio measurements for each treatment were normalized by dividing by the mean outside edge ratios for that treatment (set to 1). A summary table comprising the 10–15 unweighted per-cluster means obtained for each combination of treatment and morphological class was used for further statistical analysis. Treatment effects and differences between morphological classes were evaluated by ANOVA. Nonparametric means comparisons yielded similar results. For tests of significance, α was set to 0.05 prior to Dunn-Sidak correction for multiple comparisons (Sokal and Rohlf, 1994). Statistics were calculated using JMP IN v4.0.2 (SAS Institute).

Protein enrichments are likely to be substantially higher than our ratiometric estimates. Trade-offs between spatial resolution and signal-to-noise ratio limit the dynamic range obtainable at submicron spatial scales. Thus, our ratiometric data provide lower-bounds estimates of protein accumulation at resolution-limited sites. Light microscopic studies of other fusion systems have yielded quantitatively similar results (Roberts et al., 1999; Lang et al., 2001).

Time-Lapse Microscopy

Clusters of docked purified vacuoles or cells containing apposed vacuoles were identified, and FM 4-64, GFP, and Nomarski image sets were captured simultaneously on a BioRad MRC 1024 confocal microscope with a Zeiss Plan Apochromat 100× 1.4 NA objective. The confocal pinhole was set to relatively wide apertures to maximize signal transmission and to increase depth of field. Image analysis was performed using NIH Image and Adobe Photoshop. The images in Figure 1 have been adjusted to compensate for photobleaching, using decay constants derived from single exponential fits to the intensity data. The associated videos are not adjusted for photobleaching.

Aqueous Probe Transfer Assay

Calcein AM ester (10 μM; Molecular Probes) was loaded for 40 min at 27°C during spheroplasting, and vacuoles were isolated by flotation (Haas, 1995). Calcein loading did not affect vacuole fusion rates or sensitivity to Vam3p antibody, Gdi1p, or BAPTA (data not shown). Mixtures of unlabeled and calcein-labeled vacuoles (6 μg) were incubated (1 hr, 27°C) with no inhibitor, 5 mM BAPTA, or 67 ng/μl his_6-Sec17p (Haas and Wickner, 1996), and then mixed with 30 μl 0.6% molten low-melt agarose. Random fields were acquired on a BioRad MRC 1024 confocal microscope. For each channel, two frames were Kalman averaged. Black level was set so that background noise could be characterized, and gain was set so that more than 50% of the calcein-labeled lumens had saturated pixels (gray value $>$ 255). Pixel values $<$5 rmsd above the nonvacuole mean were defined as noise and set to zero. Typically, this noise threshold was $\sim$30 gray levels above the background mean. The signal-to-noise ratio was in all cases $>$5:1; transfer of 20% of lumenal calcein to an adjacent vacuole would have been detected.

Acknowledgments

This work was supported by National Institute of General Medical Sciences. Digital fluorescence microscopy equipment was funded by the Rippel Foundation. A.J.M. is supported by fellowship DRG-1598 of the Cancer Research Fund of the Damon Runyon-Walter Winchell Foundation. We thank Dr. Duane Compton for guidance with microscopy, Drs. Michael Sheetz, Richard Cardullo, and Jason Swedlow for advice on image analysis, Dr. Pamela Silver for the Superglow GFP variant and for hospitality, Stephanie Zimsen for guidance with statistical analysis, and Drs. Albert Haas, Thomas Sudhof, Randy Schekman, Peter Novick, and Pietro DeCamilli for insightful suggestions.

Received August 27, 2001; revised January 7, 2002.

References

Bone, N., Millar, J.B.A., Toda, T., and Armstrong, J. (1998). Regulated vacuole fusion and fission in *Schizosaccharomyces pombe*: an osmotic response dependent on MAP kinases. Curr. Biol. *8*, 135–144.

Burgoyne, R.D., and Morgan, A. (1998). Calcium sensors in regulated exocytosis. Cell Calcium *24*, 367–376.

Chernomordik, L.V., and Sowers, A.E. (1991). Evidence that the spectrin network and a nonosmotic force control the fusion product morphology in electrofused erythrocyte ghosts. Biophys. J. *60*, 1026–1037.

Conradt, B., Shaw, J., Vida, T., Emr, S.D., and Wickner, W. (1992). *In vitro* reactions of vacuole inheritance. J. Cell Biol. *119*, 1469–1479.

Conradt, B., Haas, A., and Wickner, W. (1994). Determination of four biochemically distinct, sequential stages during vacuole inheritance *in vitro*. J. Cell Biol. *126*, 99–110.

de Duve, C., and Wattiaux, R. (1966). Functions of lysosomes. Annu. Rev. Physiol. *23*, 435–492.

Denzer, K., Kleijmeer, M.J., Heijnen, H.F., Stoorvogel, W., and Geuze, H.J. (2000). Exosome: from internal vesicle of the multivesicular body to intercellular signalling device. J. Cell Sci. *113*, 3365–3374.

Dublova, I., Yamaguchi, T., Wang, Y., Sudhof, T., and Rizo, J. (2001). Vam3p structure reveals conserved and divergent properties of syntaxins. Nat. Struct. Biol. *8*, 258–264.

Eitzen, G., Will, E., Gallwitz, D., Haas, A., and Wickner, W. (2000). Sequential action of two GTPases to promote vacuole docking and fusion. EMBO J. *19*, 6713–6720.

Guo, W., Tamanoi, F., and Novick, P. (2001). Spatial regulation of the exocyst complex by Rho1 GTPase. Nat. Cell Biol. *3*, 353–360.

Haas, A. (1995). A quantitative assay to measure homotypic fusion in vitro. Methods Cell Sci. *17*, 283–294.

Haas, A., and Wickner, W. (1996). Homotypic vacuole fusion requires Sec17p (yeast α-SNAP) and Sec18p (yeast NSF). EMBO J. *15*, 3296–3305.

Haas, A., Conradt, B., and Wickner, W. (1994). G-protein ligands inhibit *in vitro* reactions of vacuole inheritance. J. Cell Biol. *126*, 87–97.

Haas, A., Scheglmann, D., Lazar, T., Gallwitz, D., and Wickner, W. (1995). The GTPase Ypt7p of *Saccharomyces cerevisiae* is required on both partner vacuoles for the homotypic fusion step of vacuole inheritance. EMBO J. *14*, 5258–5270.

Hall, A. (1998). Rho GTPases and the actin cytoskeleton. Science *279*, 509–514.

Hirsch, J.G., Fedorko, M.E., and Cohn, Z.A. (1968). Vesicle fusion and formation at the surface of pinocytic vacuoles in macrophages. J. Cell Biol. *38*, 629–633.

Kahana, J.A., and Silver, P. (1998). The uses of green fluorescent protein in yeasts. In Green Fluorescent Protein: Properties, Applications, and Protocols, M. Chalfie and S. Kain, eds. (New York: Wiley-Liss, Inc.), pp 139–151.

Lang, T., Bruns, D., Wenzel, D., Riedel, D., Holroyd, P., Thiele, C., and Jahn, R. (2001). SNAREs are concentrated in cholesterol-dependent clusters that define docking and fusion sites for exocytosis. EMBO J. *20*, 2202–2213.

Longtine, M.S., McKenzie, A., Demarini, D.J., Shah, N.G., Wach, A., Brachat, A., Philippsen, P., and Pringle, J.R. (1998). Additional modules for versatile and economical PCR-based gene deletion andmodification in *Saccharomyces cerevisiae*. Yeast *14*, 953–961.

Mayer, A., and Wickner, W. (1997). Docking of yeast vacuoles is catalyzed by the Ras-like GTPase Ypt7p after symmetric priming by Sec18p (NSF). J. Cell Biol. *136*, 307–317.

Mayer, A., Wickner, W., and Haas, A. (1996). Sec18p (NSF)-driven release of Sec17p (α-SNAP) can precede docking and fusion of yeast vacuoles. Cell *85*, 83–94.

Miller, F., and Palade, G.E. (1964). Lytic activities in renal protein absorption droplets. J. Cell Biol. *23*, 519–522.

Nichols, B.J., Ungermann, C., Pelham, H.R.B., Wickner, W.T., and

Haas, A. (1997). Homotypic vacuolar fusion mediated by t- and v-SNAREs. Nature *387*, 199–202.

Novick, P., and Zerial, M. (1997). The diversity of Rab proteins in vesicle transport. Curr. Op. Cell Biol. *9*, 496–504.

Odorizzi, G., Babst, M., and Emr, S.D. (1998). Fab1p PtdIns(3)P 5-kinase function essential for protein sorting in the multivesicular body. Cell *95*, 847–858.

Olbricht, K., Plattner, H., and Matt, H. (1984). Synchronous exocytosis in Paramecium cells. II. Intramembranous changes analysed by freeze-fracturing. Exp. Cell Res. *151*, 14–20.

Pan, X., and Goldfarb, D.S. (1998). YEB3/VAC8 encodes a myristoylated armadillo protein of the *Saccharomyces cerevisiae* vacuolar membrane that functions in vacuole fusion and inheritance. J. Cell Sci. *111*, 2137–2147.

Peters, C., and Mayer, A. (1998). Ca^{2+}/calmodulin signals the completion of docking and triggers a late step of vacuole fusion. Nature *396*, 575–580.

Peters, C., Andrews, P.D., Stark, M.J.R., Cesaro-Tadic, S., Glatz, A., Podtelejnikov, A., Mann, M., and Mayer, A. (1999). Control of the terminal step of intracellular membrane fusion by protein phosphatase 1. Science *285*, 1084–1087.

Peters, C., Bayer, M.J., Buhler, S., Andersen, J.S., Mann, M., and Mayer, A. (2001). Trans-complex formation by proteolipid channels in the terminal phase of membrane fusion. Nature *409*, 581–588.

Price, A., Wickner, W., and Ungermann, C. (2000a). Vacuole protein sorting (VPS) proteins needed for transport vesicle budding from the Golgi are also required for the docking step of homotypic vacuole fusion. J. Cell Biol. *148*, 1223–1230.

Price, A., Seals, D., Wickner, W., and Ungermann, C. (2000b). The docking stage of yeast vacuole fusion requires the transfer of proteins from a *cis*-SNARE complex to a Rab/Ypt protein. J. Cell Biol. *148*, 1231–1238.

Roberts, R.L., Barbieri, M.A., Pryse, K.M., Chua, M., Morisaki, J.H., and Stahl, P.D. (1999). Endosome fusion in living cells overexpressing GFP-rab5. J. Cell Sci. *112*, 3667–3675.

Sato, T.K., Rehling, P., Peterson, M.R., and Emr, S.D. (2000). Class C Vps protein complex regulates vacuolar SNARE pairing and is required for vesicle docking/fusion. Mol. Cell *6*, 661–671.

Seals, D., Eitzen, G., Margolis, N., Wickner, W., and Price, A. (2000). A Ypt/Rab effector complex containing the Sec1 homolog Vps33p is required for homotypic vacuole fusion. Proc. Natl. Acad. Sci. USA *97*, 9402–9407.

Sokal, R.R., and Rohlf, F.J. (1994). Biometry: The Principles and Practice of Statistics in Biological Research, 3rd ed. (New York: W.H. Freeman).

Sudhof, T.C., and Rizo, J. (1996). Synaptotagmins: C2-domain proteins that regulate membrane traffic. Neuron *17*, 379–388.

Ungermann, C., and Wickner, W. (1998). Vam7p, a vacuolar SNAP-25 homolog, is required for SNARE complex integrity and vacuole docking and fusion. EMBO J. *17*, 3269–3276.

Ungermann, C., Nichols, B.J., Pelham, H.R.B., and Wickner, W. (1998a). A vacuolar v-t-SNARE complex, the predominant form in vivo and on isolated vacuoles, is disassembled and activated for docking and fusion. J. Cell Biol. *140*, 61–69.

Ungermann, C., Sato, K., and Wickner, W. (1998b). Defining the functions of *trans*-SNARE pairs. Nature *396*, 543–548.

Ungermann, C., von Mollard, G.F., Jensen, O.N., Margolis, N., Stevens, T., and Wickner, W. (1999a). Three v-SNAREs and two t-SNAREs, present in a pentameric cis-SNARE complex on isolated vacuoles, are essential for homotypic fusion. J. Cell Biol. *145*, 1435–1442.

Ungermann, C., Wickner, W., and Xu, Z. (1999b). Vacuole acidification is required for *trans*-SNARE pairing, LMA1 release, and homotypic fusion. Proc. Natl. Acad. Sci. USA *96*, 11194–11199.

Ungermann, C., Price, A., and Wickner, W. (2000). A new role for a SNARE protein as a regulator of the Ypt7/Rab-dependent stage of docking. Proc. Natl. Acad. Sci. USA *97*, 8889–8891.

Veit, M., Laage, R., Dietrich, L., Wang, L., and Ungermann, C. (2001). Vac8p-release from the SNARE complex and its palmitoylation are coupled and essential for vacuole fusion. EMBO J. *20*, 3145–3155.

Wang, L., Ungermann, C., and Wickner, W. (2000). The docking of primed vacuoles can be reversibly arrested by excess Sec17p (α-SNAP). J. Biol. Chem. *275*, 22862–22867.

Wang, Y.-X., Kauffman, E.J., Deux, J.E., and Weisman, L.S. (2001). Fusion of docked membranes requires the armadillo repeat protein Vac8p. J. Biol. Chem. *276*, 35133–35140.

Wickner, W., and Haas, A. (2000). Yeast vacuole fusion: a window on organelle trafficking mechanisms. Annu. Rev. Biochem. *69*, 247–275.

Wurmser, A.E., Sato, T.K., and Emr, S.D. (2000). New component of the vacuolar class C-Vps complex couples nucleotide exchange on the Ypt7 GTPase to SNARE-dependent docking and fusion. J. Cell Biol. *151*, 551–562.

Xu, Z., Sato, K., and Wickner, W. (1998). LMA1 binds to vacuoles at Sec18p (NSF), transfers upon ATP hydrolysis to a t-SNARE (Vam3p) complex, and is released during fusion. Cell *93*, 1125–1134.

Yamamoto, A., DeWald, D.B., Boronenkov, I.V., Anderson, R.A., Emr, S.D., and Koshland, D. (1995). Novel PI(4)P 5-kinase homologue, Fab1p, essential for normal vacuole function and morphology in yeast. Mol. Biol. Cell *6*, 525–539.

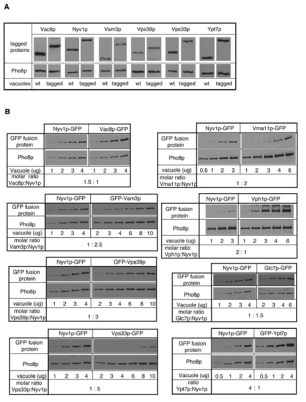
A
Vac8p
Nyv1p
Vam3p
Vps39p
Vps33p
Ypt7p
tagged proteins
Pho8p
vacuoles
wt
tagged
B
Nyv1p-GFP
Vac8p-GFP
GFP fusion protein
Pho8p
Vacuole (ug)
molar ratio Vac8p:Nyv1p
1 2 3 4 1 2 3 4
1.5 : 1
Nyv1p-GFP
Vma11p-GFP
0.5 1 2 3 1 2 3 4 6
1 : 2
Nyv1p-GFP
GFP-Vam3p
1 2 3 4 2 3 4 6 8 10
1 : 2.5
Nyv1p-GFP
Vph1p-GFP
1 2 3 1 2 3 4 6
2 : 1
Nyv1p-GFP
GFP-Vps39p
1 2 3 4 2 3 4 6 8 10
1 : 3
Nyv1p-GFP
Glc7p-GFP
1 2 3 4 2 3 4 6
1 : 1.5
Nyv1p-GFP
Vps33p-GFP
1 2 3 4 2 3 4 6 8 10
1 : 5
Nyv1p-GFP
GFP-Ypt7p
0.5 1 2 4 0.5 1 2 4
4 : 1

A

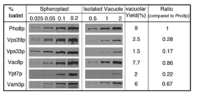
% loaded
Spheroplast
0.025 0.05 0.1 0.2
Isolated Vacuole
0.5 1 2
Vacuolar Yield(%)
Ratio (compared to Pho8p)
Pho8p
9
1
Vps39p
2.5
0.28
Vps33p
1.5
0.17
Vac8p
7.7
0.86
Ypt7p
2
0.22
Vam3p
6
0.67

B

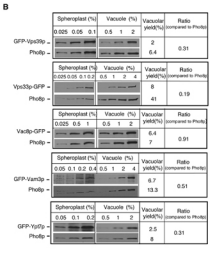
Spheroplast (%)
Vacuole (%)
Vacuolar yield(%)
Ratio (compared to Pho8p)
0.025 0.05 0.1
0.5 1 2
GFP-Vps39p
Pho8p
2
6.4
0.31
0.025 0.05 0.1 0.2
0.5 1 2 4
Vps33p-GFP
8
41
0.19
0.025 0.5 1
0.5 1 2
Vac8p-GFP
6.4
7
0.91
0.05 0.1 0.2 0.4
0.5 1 2 4
GFP-Vam3p
6.7
13.3
0.51
0.05 0.1 0.2
0.5 1 2
GFP-Ypt7p
2.5
8
0.31

Wang et al., Figure S3

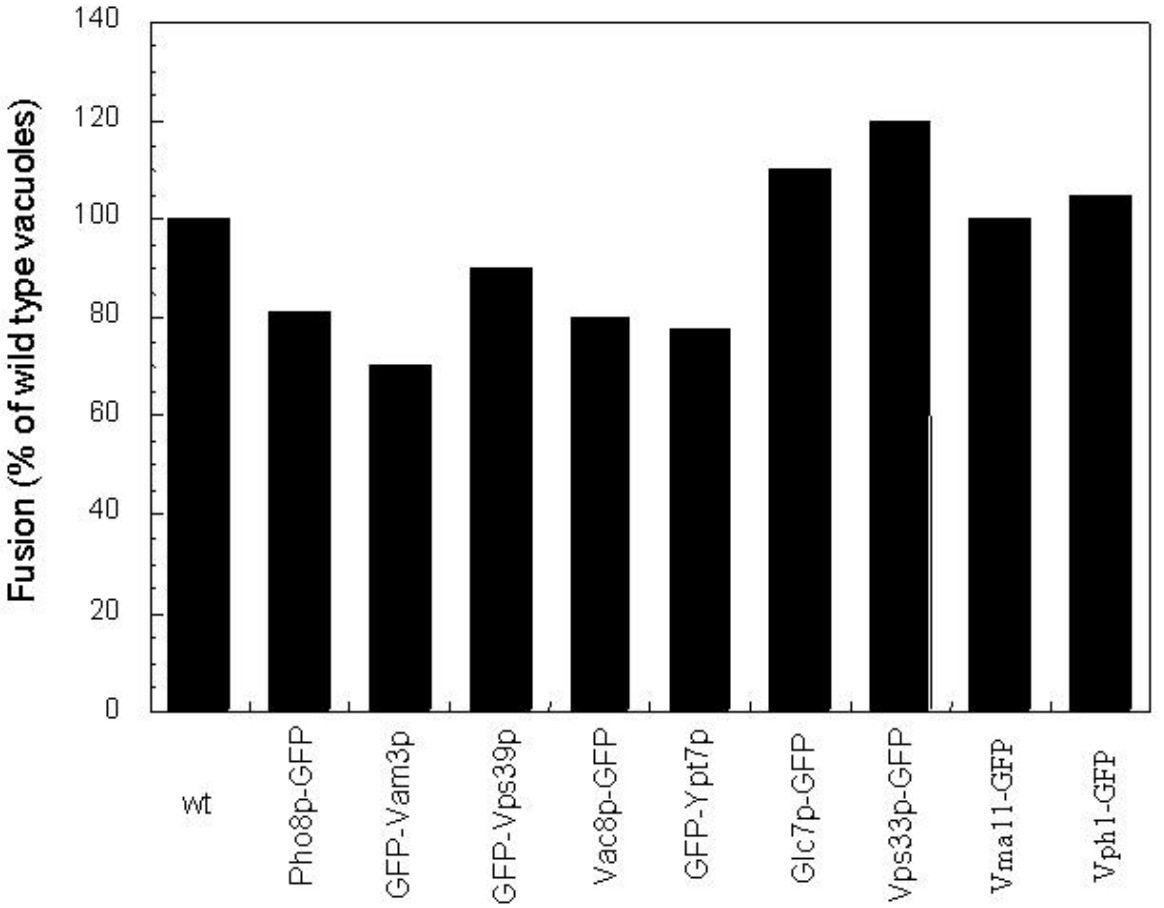

Supplemental Table 1. Yeast Strains Expressing GFP-Tagged Proteins

GFP-Tagged Strains	GFP Tag Location	Genotype
Pho8-GFP:BJ2168	C terminus	*MATα, leu2-3,112, trp1-Δ1, ura3-52, prb1-1122, pep4-3, pcr1-407 PHO8-GFP (TRP1)*
Pho8-GFP:SEY6210		*MATα leu2-3 leu2-112 ura3-52 his3-Δ200 trp1-Δ901 lys2-801 suc2-Δ9 pep4::HIS3 PHO8-GFP (TRP1)*
Vac8-GFP:BJ2168	C terminus	*MATα, leu2-3,112, trp1-Δ1, ura3-52, prb1-1122, pep4-3, pcr1-407 VAC8-GFP (TRP1)*
Vac8-GFP:DKY6281		*MATα leu2-3 leu2-112 ura3-52 his3-Δ200 trp1-Δ901 lys2-801 suc2-Δ9 pho8::TRP1 VAC8-GFP (HIS3)*
GFP-Vam3:BJ3505	N terminus	*MATαpep4::HIS3 prb1-Δ1.6R HIS3 lys2-208 trp1-Δ1 ura3-52 vam3::TRP1 pGFP-VAM3*
GFP-Vam3:SEY6210	N terminus	*MATα leu2-3 leu2-112 ura3-52 his3-Δ200 trp1-Δ901 lys2-801 suc2-Δ9 vam3::HIS3 pGFP-VAM3*
Vps33-GFP:BJ2168	C terminus	*MATα, leu2-3,112, trp1-Δ1, ura3-52, prb1-1122, pep4-3, pcr1-407 VPS33-GFP (TRP1)*
Vps33-GFP:DKY6281		*MATα leu2-3 leu2-112 ura3-52 his3-Δ200 trp1-Δ901 lys2-801 suc2-Δ9 pho8::TRP1 VPS33-GFP (HIS3)*
Glc7-GFP:BJ2168	C terminus	*MATα, leu2-3,112, trp1-Δ1, ura3-52, prb1-1122, pep4-3, pcr1-407 GLC7-GFP (TRP1)*
Glc7-GFP:DKY6281		*MATα leu2-3 leu2-112 ura3-52 his3-Δ200 trp1-Δ901 lys2-801 suc2-Δ9 pho8::TRP1 GLC7-GFP (HIS3)*
GFP-Vps39:BJ3505	N terminus	*MATαpep4::HIS3 prb1-Δ1.6R HIS3 lys2-208 trp1-Δ1 ura3-52 vam6::URA3 pGFP-Vps39p*
GFP-Vps39:SEY6210		*MATαleu2-3 leu2-112 ura3-52 his3-Δ200 trp1-Δ901 lys2-801 suc2-Δ9 vam6::HIS3 pGFP-Vps39p*
GFP-Ypt7:BJ3505	N terminus	*MATαpep4::HIS3 prb1-Δ1.6R HIS3 lys2-208 trp1-Δ1 ura3-52 ypt7::URA3 pGFP-YPT7*
GFP-Ypt7:SEY6210		*MATαleu2-3 leu2-112 ura3-52 his3-Δ200 trp1-Δ901 lys2-801 suc2-Δ9 ypt7::HIS3 pGFP-YPT7*
Vph1-GFP:SEY6210	C terminus	*MATα leu2-3 leu2-112 ura3-52 his3-Δ200 trp1-Δ901 lys2-801 suc2-Δ9 pep4::HIS3 VPH1-GFP(TRP1)*
Vma11-GFP:SEY6210	C terminus	*MATα leu2-3 leu2-112 ura3-52 his3-Δ200 trp1-Δ901 lys2-801 suc2-Δ9 pep4::HIS3 VMA11-GFP(TRP1)*

Supplemental Table 2. Oligonucleotides for C Terminus Tagging and Gene Knockout

Pho8-F2	TAG TGA AGT ACA ACA TTA TGA CGA ATA CTA CCA TGA GTT GAC CAA CCG GAT CCC CGG GTT AAT TAA
Pho8-R1	TAA CGT ATT AAA TAA TAT GTG AAA AAA GAG GGA GAG TTA GAT AGG AGA ATT CGA GCT CGT TTA AAC
Vac8-F2	GGA ATT GTA TAA TAT TAC TCA ACA GAT TTT ACA ATT TTT ACA TCG GAT CCC CGG GTT AAT TAA
Vac8-R1	TTG ATA AAA ATT ATA ATG CCT AGT CCC GCT TTT GAA GAA AAG AAT TCG AGC TCG TTT AAA C
Ypt7-F1	CTT ATC CAT ATA GAA ACC CCT TCT GTA TCA ATT CAA ATT AAG TGC GGA TCC CCG GGT TAA TTA A
Ypt7-R1	CGC TAT AAA GGA TTA CAT AAT AGA AGA TAC AAT TAA GTA GTA CAG CGA ATT CGA GCT CGT TTA AAC
Vps39-F1	ATT GAT CAG CAA AAA CCC TTC AAA ATA TCA ATT TAT ACC AAA AAT TAA CGG ATC CCC GGG TTA ATT AA
Vps39-R1	ATA AGA AAT ACT AAC AAC AAT AAC AGC AGC TGT TAA GGG ATC GAA TTC GAG CTC GTT TAA AC
Vps33-F2	CCG ATG GCT TGA TCA ATG GCA CAA GGA TCA TGA ACT CTA TAT CTC GGA TCC CCG GGT TAA TTA A
Vps33-R1	GCA CAT TTG CAT ATA CAA AAA ATT AAC AAA TCT ATC ATA TAA TAA GAA TTC GAG CTC GTT TAA AC
Vam3-F1	GCA TTA ACA AAT TGG CCA ACT AAT ATC CAC TGC AGA AAG TTG AGA TTC GGA TCC CCG GGT TAA TTAA
Vam3-F2	ATA ATA GTT GTG TGC ATG GTG GTA TTG CTT GCT GTA TTA AGT CGG ATC CCC GGG TTA ATT AA
Vam3-R1	ATT GGG TCT ACC AGA AAG TCT GTG CTC AAT GCG CGT TTA AGG GAA TTC GAG CTC GTT TAA AC
Vam7-F1	AAC AAA AAC AAA AAC AAT AAA GTC ATA TAA GGG TTG ATA ATT GAT ATT GCG GAT CCC CGG GTTAATTAA
Vam7-R1	CAA ATA TAC TCT CAG GAT TTG TAA CCC GGA TAG TAA CTC ATT AAT GAA TTC GAG CTC GTT TAA AC
Glc7-F2	CCA GCC CAA AAA AGT CTA CCA AGG CAA GCT GGG GGT AGA AAG AAA AAA CGG ATC CCCGGGTTAATTAA
Glc7-R1	GTA TTT TCC TTT TTA AAC TTT GAT TTA GGA CGT GAA TCT ATG AAT TCG AGC TCG TTT AAA C
Vph1-F2	AGA CAT GGA AGT CGC TGT TGC TAG TGC AAG CTC TTC CGC TTC AAG CCG GAT CCC CGG GTT AAT TAA
Vph1-R1	AAT GAA GTA CTT AAA TGT TTC GCT TTT TTT AAA AGT CCT CAA AAT GAA TTC GAG CTC GTT TAA AC
Vma11-F2	TGG TAT GAT TGT AGC TTT GAT TTT GAA CAC TAG AGG CTC TGA ACG GAT CCC CGG GTT AAT TAA
Vma11-R1	TGA GAA AAA ATT TTT TTA TTG TAA TTA TTT TTT TTT TTT AAA CTT TTG ACG AAT TCG AGC TCG TTT AAA C

F1 forward primer for gene deletion: the gene-specific sequences are chosen to end just upstream of the start codon.
F2 forward primer for C terminus tagging: the gene-specific sequences are chosen to end just upstream of the stop codon, preserving the reading frame.
R1 reverse primer for C terminus tagging: the gene-specific sequences are chosen to end just downstream of the stop codon.

Supplemental Table 3. Integrating Plasmids Constructed for N Terminus Tagging

Plasmids	Description	Oligonucleotides for Constructing Fusion Proteins Expressed under Their Native Promoters
pGFP-Vps39	GFP -Vps39 fusion, integrating vector YIPlac211/TRP1	Vam6-down-5'-XbaI: TGC TCT AGA TCA CAT CAC GTA TTC GCG CCT GCG ACA Vam6-down-3'-PstI: AAC TGC AGG CAC TGA CAA GTG TTT TCC CTT GAT TTA CG GFP-5'-NheI: CTA GCT AGC ATG GCT AGC AAA GGA GAA GAA GFP-3'-NheI: CTA GCT AGC GCA GCC GGA TCC TTT GTA TAG
pGFP-YPT7	GFP -Ypt7 fusion, integrating vector PRS304/TRP1	Ypt7-up-5'-KpnI: CGG GGT ACC GCG TGA ACA ATC GGA GCA AAG AC Ypt7-up-3'-EcoRI: CCG GAA TTC CAC TTA ATT TGA ATT GAT ACA GAA GGG G Ypt7-5'-PstI: AAA ACT GCA GTC TTC TAG AAA AAA AAA TAT TTT GAA AG Ypt7-3'-XhoI: CCG CTC GAG GGT AGC CAG AAC TTC TCA TCA ACA Ypt7-down-5'-XhoI: CCG CTC GAG ACT ATG GCG GTA TAA GTT TCT CCC GCC TTG Ypt7-down-3'-NotI: ATA AGA ATG CGG CCG CGG TGC CCA TTG GAA GAG TGA CAAC GFP-5'-EcoRI: CCG GAA TTC ATG GCT AGC AAA GGA GAA GAA GFP-3'-PstI: AAA ACT GCA GGC AGC CGG ATC CTT TGT ATA GTT C
pGFP-VAM3	GFP-GFP-Vam3 fusion, Integrating vector PRS306/URA	Vam3-up-5'-XhoI: CCG CTC GAG GAT CAA GAG GAT TCA TTG GT Vam3-up-3'-EcoRI: CCG GAA TTC AAT CTC AAC TTT CTG CAG TG Vam3-5'- HindIII: CGC GCG AAG CTT ATG TCC TTT TTC GAC ATC GAA GCA Vam3-3'- KpnI: CGG GGT ACC GGG CCC ACA AGG TTC ATT TAG GFP-5'-EcoRI: CCG GAA TTC ATG GCT AGC AAA GGA GAA GAA GFP-3'-XbaI: TGC TCT AGA GCA GCC GGA TCC TTT GTA TAG TTC GFP-5'-XbaI: GCT CTA GAA TGG CTA GCA AAG GAG AAG AA GFP-3'-HindIII: CCC AAG CTT GCA GCC GGA TCC TTT GTA TAG TTC

For each construct, the promoter region was cloned into the integrating vector as specified, followed by the GFP module, which was fused in-frame to the 5' end of the gene. "UP" refers to the oligonucleotides for upstream promoter regions, and "down" was used to describe oligonucleotides for regions following open reading frames.